Practical Considerations in Precise Calibration of a Low-cost MEMS IMU for Road-Mapping Applications

Ashkan Amirsadri, Jonghyuk Kim, Lars Petersson, Jochen Trumpf

***Abstract*—This paper addresses the theoretical and experimental development of a calibration scheme to overcome the intrinsic limitations of a low-cost Micro-Electrical-Mechanical System (MEMS) based Inertial Measurement Unit (IMU). The two-stage calibration algorithm was developed and tested successfully on a six-degree of freedom prototype MEMS IMU to determine the deterministic and stochastic errors of the sensor. This paper makes use of artificial observations known as pseudo-velocity measurements resulting from a specific scheme of rotation to calibrate the IMU in the laboratory environment. The proposed structure is then modified and utilised as a basis for the IMU's error estimation in outdoor navigation applications. For this purpose, the designed calibration method is applied to an integrated GPS/MEMS IMU system, showing improved navigational and road sign positioning performance in a test vehicle.**

***Index Terms*—Bias, Scale-Factor Error, Static Calibration, Dynamic Calibration, the Extended Kalman Filter (EKF).**

I. Introduction

The last two decades have witnessed an increasing trend towards the use of navigation and positioning technologies in land vehicle applications. The demand for high quality navigation information on one hand and the well-known limitations of the Global Positioning System (GPS) on the other hand have driven the research into employment of Inertial Navigation Systems (INS) in positioning and mapping applications. Probably one of the most widely used inertial sensor assemblies is the Inertial Measurement Unit (IMU). A tri-axial IMU, like the one implemented in this work, includes a triad of gyroscopes and accelerometers, all placed in an orthogonal arrangement with respect to each other.

In spite of their widespread utilisation, the high cost and complexity of traditional inertial navigation systems create some constraints on their use in general purpose civilian applications. The advent of Micro-Electrical-Mechanical Systems (MEMS) has enabled the manufacturing of low-cost inertial sensors. MEMS-based IMUs have proved their use in a myriad of applications from robotics to integrated navigation systems. These sensors are capable of providing reasonably accurate navigation data over short intervals of time. Nevertheless, the major challenge in dealing with them is their notorious error characteristic which leads to degraded performance in the long term [1]. Consequently, determining the associated errors (such as noises, biases, drifts and scale factor instabilities) becomes indispensable in the utilisation of these sensors in real-world navigation applications.

The work in this paper is strongly motivated by a project called AutoMap which aims at developing cost effective methods for automatic creation of digital maps [2]. The project exploits computer vision algorithms for road sign extraction from video footage captured by land vehicles. The AutoMap project requires continuous positioning information of the fleet vehicle in order to localise the detected landmarks. For this purpose, inertial sensors are used alongside the GPS to obtain synergetic observation effects. The utilisation of low-cost MEMS IMUs enables the development of data collection sensor platforms at a reasonable cost. Consequently, the study and calibration of the MEMS IMU in this work is of vital importance to the future development of the AutoMap technology.

Over the years, several calibration techniques have been developed in different works to address the problem of accumulative errors presented in inertial sensors. Grewal et al. [3] and Foxlin & Naimark [4] designed a Kalman filter with precise maneuvers to calibrate low-cost IMU sensors for less demanding applications. Their methods have difficulties generating accurate external calibration values such as bias and scale factor errors and they often require costly and high-precision equipment which may not be available to researchers for general orientation measurement applications. Nebot & Durrant-Whyte [5] implemented an algorithm for online initial calibration and alignment of an IMU with six degrees-of-freedom (DoF) for land vehicle navigation applications. Kim & Golnaraghi [6] studied a calibration process using an optical tracking system. Park & Gao [7] and Syed et al. [8] investigated the lab calibration of MEMS-based IMUs by developing a turn table test procedure. Hall & Williams [9] developed an electromechanical system for automated calibration of IMUs using GPS antennas. Titterton & Weston [10], Farrel [11] and Shin & Sheimy [12] used a velocity matching alignment method where the attitude of the IMU was being initialised by the GPS velocity information. A common finding of the majority of prior works on calibration is that they do not account for the time-varying errors associated with inertial sensors. We will address this issue by constantly and continuously estimating and compensating for the IMU's stochastic errors. Although online error estimation and fault-

This work is supported by the *Australian National University (ANU)* and *NICTA*. NICTA is funded by the Australian Government as represented by the Department of Broadband, Communications and the Digital Economy and the Australian Research Council through the ICT Centre of Excellence program.

A. Amirsadri (ashkan.amirsadri@anu.edu.au) and J. Kim are with the ANU and NICTA. L. Petersson is with NICTA and is an adjunct to the ANU. J. Trumpf is with the ANU.

detection techniques were previously investigated in other publications such as [13], the context in which they appear in this work is different in implementation and application. The method in [13] investigates the fault detection of IMU and GPS in a GPS/INS fusion system for outdoor applications. However, unlike our method, it does not address the stand-alone calibration of the inertial sensors for removing the time-varying errors in the lab environment.

This paper provides a systematic framework for both lab and in-field calibration of a 6-DoF MEMS-based inertial measurement unit. The proposed calibration scheme is comprised of two distinct phases which are implemented sequentially. Firstly, fixed errors are removed from the stationary IMU during a designed laboratory test in a process referred to as static calibration. Secondly, the extended Kalman filter (EKF) is utilised in a context known as dynamic calibration to estimate the time-varying errors. An intuitive concept called a pseudo-measurement based approach was taken to tackle the dynamic calibration problem in the lab environment. The pseudo-measurement method is closely related, but not identical to the concept of zero velocity update (ZUPT) in [14] and [15]. ZUPT is often used for outdoor applications and it involves performing calibration and resetting the sensor's errors while the vehicle is stationary. However, as will be seen later in this paper, the pseudo-measurement methodology dynamically and continuously estimates and removes the time-varying errors of inertial sensors. In addition, the relaxed rotational scheme in the lab environment, which will be described later, provides a more general type of motion for the calibration experiment compared to the ZUPT method.

Although the pseudo-measurement concept is mainly designed for lab calibration, it can easily be expanded to incorporate GPS measurements to calibrate low-grade IMUs in outdoor navigation applications. Unlike [7], [8], [16], the calibration solution described here is independent of any advanced equipment such as turn tables and it does not require precise maneuvers explained in [3], [4]. It provides a simpler operational solution than [14], [17] in that it does not require the frequent stoppage of the vehicle to perform calibration. Moreover, in contrast to [18], [19] it does not require a thermal model and a thermal calibration of the sensor.

The rest of this paper is arranged as follows. Section II starts with a brief overview on the calibration procedure and providing the preliminary definitions. Subsection II-A explains a methodical solution for static calibration of an IMU. Section II-B employs the state space representation to formulate the dynamic calibration algorithm in the extended Kalman filtering context. This section introduces the pseudo-measurement concept and a specific scheme of rotational movement as the main contribution of this paper. Section III provides the IMU calibration results followed by the results of the GPS/MEMS-based IMU fusion system. This system is a real-world navigation application of the pseudo-measurement based calibration framework provided earlier. Finally, the conclusions are drawn from the results in Section IV.

II. Calibration Scheme

Calibration is widely defined as the process of comparing instrument outputs with known reference information. In this process, the coefficients are determined that force the output to agree with the reference information for any range of output values. The error characteristic of MEMS components is often highly nonlinear and temperature dependent. In addition, MEMS-based IMUs are typically not compensated for errors such as biases and scale factors. To achieve the desired accuracy, it is therefore crucial to model the dominating errors and analyse their effects in navigation applications.

Accelerometer bias is defined as an offset in the output that varies randomly from time to time after removing the gravitational term. Gyro bias offset is the measured angular velocity when no rotational motion is present. On the other hand, the scale factor errors of the accelerometer and gyro are errors which are proportional to the sensed quantities. The errors caused by the bias and scale factor in the inaccurate sensor reading accumulate with time and will subsequently lead to the systematic error known as the integration drift in the velocity, position and attitude provided by the unit. The calibration model used in this paper is a simple linear model where the scale factor (S_A) and bias (β_A) are, respectively, the multiplicative and additive factors of the generic variable A. That is

$$A(t) = S_A \tilde{A}(t) + \beta_A(t) \tag{1}$$

where A denotes the real value of the quantity which is being calibrated, and $\tilde{A}$ is the direct reading from the sensor. Other error sources such as axis misalignment errors are not taken into account in this work[1]. Interested readers are referred to [13] and [21] for axis misalignment estimation.

The measurement errors in an IMU can be categorised into deterministic and stochastic errors [22]. The term deterministic errors refers to fixed biases and scale factor errors. In contrast, stochastic errors vary randomly from time to time which is an intrinsic nature of MEMS sensors. In this paper, the calibration is performed through two consecutive steps. At first, the deterministic errors presented in the raw sensor measurements will be compensated using controlled experimental methods to calculate the *conditioned* inertial quantities. This is called the static calibration procedure. The method employs a variation of the six-position static and rate tests which are discussed in different works [8], [10]. In the second stage, the conditioned accelerations and angular rates from the first step are fed into the designed calibration module as inputs. This structure estimates the stochastic errors presented in the sensor. This step is referred to as the dynamic calibration. The pseudo-measurement concept provided by a relaxed rotational movement is introduced in this phase as a tool for estimating the time-varying errors of the implemented IMU during a mission.

A. Static Calibration

The deterministic type of errors in an IMU can usually be

[1]Since, in the MEMS quality sensor under study, all components are assembled in a single, automated PCB assembly step, misalignment errors can be kept to a minimum.

determined in controlled laboratory tests. Several procedures (e.g. [23], [24], [25]) have been proposed in the literature to remove the fixed errors of inertial sensors. Typically, for obtaining the biases of inertial sensors, the simplest method is to measure the output reading while the sensor is stationary. The methodology which has been used in this paper is described here[2]. The scale factor of the gyro is determined by using the information from the sensor's data sheet. Using the employed Analog-Digital Converter (ADC) specifications and sensor's sensitivity, a rough estimate, S_{0g}, of the scale factor is calculated:

$$S_{0g} = 2^{(n_b-1)}(\frac{V_{\rm ref}}{S_{\rm gyro}}) \tag{2}$$

where $V_{\rm ref}$, $S_{\rm gyro}$ and n_b are the ADC reference voltage, the gyroscope's sensitivity and the number of ADC bits respectively. After taking into account the calculated scale factor, the bias value, $\beta_{0\rm g}$, is simply determined using the average value of gyro reading over a sufficiently large period (e.g. 2 minutes) so that Equation (1) leads to a zero value for a static IMU (a gyro at rest experiences an angular rotation equal to the Earth rotation rate, which is considered negligible for our application). Therefore,

$$\beta_{0\rm g} = -S_{0\rm g}\tilde{\omega}_{\rm avg} \tag{3}$$

where $\tilde{\omega}_{\rm avg}$ is the average sensor reading for angular rate and $\beta_{0\rm g}$ and $S_{0\rm g}$ denote the gyro's constant bias and scale factor, respectively.

Determining the unknown errors of an accelerometer is more subtle than for a gyro. In this paper, the Earth's gravity is used as a physical standard for calibrating the IMU. An accelerometer at rest on the Earth's surface will indicate $1g$ along the vertical axis,

$$\overrightarrow{a_x} + \overrightarrow{a_y} + \overrightarrow{a_z} = \overrightarrow{g} \tag{4}$$

Taking the ℓ^2 Norm of Equation (4) yields:

$$\sqrt{||\overrightarrow{a_x}||^2 + ||\overrightarrow{a_y}||^2 + ||\overrightarrow{a_z}||^2} = g \tag{5}$$

Similar to the structure of Equation (1), we define the following equation for each axis:

$$\bar{a} = S_{0a}\tilde{a}_{\rm avg} + \beta_{0a} \tag{6}$$

where $\tilde{a}_{\rm avg}$ denotes the average sensor reading and $\bar{a}$ is the resulting conditioned acceleration after compensating for the deterministic bias $\beta_{0\rm a}$ and scale factor $S_{0\rm a}$. Substituting the above equations into Equation (5) and squaring both sides of the equation yields

$$\begin{aligned}(S_{0\rm a,x}\tilde{a}_{\rm x,avg} + \beta_{0\rm a,x})^2 + \\ + (S_{0\rm a,y}\tilde{a}_{\rm y,avg} + \beta_{0\rm a,y})^2 + \\ + (S_{0\rm a,z}\tilde{a}_{\rm z,avg} + \beta_{0\rm a,z})^2 = g^2\end{aligned} \tag{7}$$

In theory, at least 6 equations are required to solve for the 6 unknown errors of Equation (7). In this work, to be prudent, 12 equations are formed by placing the IMU at 12 different tilt angles, and measuring the accelerations while the sensor is at rest. At each tilt angle, the corresponding reading for each axis is measured and averaged over a random period of time. The average values are then fed into Equation (7) to constitute the required set of equations. By taking advantage of regression analysis and curve fitting techniques on the obtained polynomials, the unknown errors of the accelerometer can be successfully computed.

B. Dynamic Calibration

Due to the nature of low-cost MEMS inertial units, the deterministic errors from Section II-A tend to vary from time to time. Drifts in angle measurements pertaining to the gyro errors, cause the gravity vector to be incorrectly subtracted from the acceleration vector, producing a virtual bias in the predicted acceleration. On the other hand, changes in the environmental conditions, especially the ambient temperature can change the bias and scale factor values. These errors are integrated into progressively larger errors in velocity, which are accumulated into even greater errors in position. It is well known that the bias terms affect the estimated velocity and attitude linearly with time, while they affect the estimated position quadratically [26]. For these reasons, the MEMS-based IMU sensors need to be calibrated frequently during a mission to avoid the accumulation of error and the integration drift phenomena.

The purpose of the designed dynamic calibration process is to statistically estimate the stochastic errors such as turn-on bias and in-run bias, by augmenting them into the state of a stochastic observer [27]. The EKF is used in this paper as the nonlinear state estimator to determine the IMU's stochastic errors. This structure receives a set of measured data from the IMU and estimates the unknown biases and scale factors of the components embedded in the sensor. However, prior to the implementation, the fixed errors are removed from the raw measurements using the static calibration procedure explained in Section II-A. Therefore,

$$\bar{a}(t) = S_{0\rm a}\tilde{a}(t) + \beta_{0\rm a} \tag{8}$$

$$\bar{\omega}(t) = S_{0\rm g}\tilde{\omega}(t) + \beta_{0\rm g} \tag{9}$$

where similar to the notation used in Equation (6), $\bar{a}$ and $\bar{\omega}$ denote the statically conditioned IMU measurements after the removal of deterministic errors. For the dynamic calibration, the acceleration and angular velocity equations for each axis are defined as[3]

$$a^b(t) = \left(1 + S_a^b(t)\right)\bar{a}(t) + \beta_a^b(t) \tag{10}$$

$$\omega^b(t) = \left(1 + S_g^b(t)\right)\bar{\omega}^b(t) + \beta_g^b(t). \tag{11}$$

The two previous equations link the conditioned values $\bar{a}$ and $\bar{\omega}$ from (8) and (9) to the real acceleration and angular

[2]Expert readers may skip the static calibration section.

[3]This is the model which is used for the dynamic calibration. Note that Equations (8) and (9) are related to the static calibration phase and should not be confused with Equations (10) and (11) introduced here.

rate values in the body-fixed frame (a^b and ω^b). The t index is used to represent the time-varying nature of the error terms. However, for the sake of simplicity in the notation, continuous or discrete time index (t and k) of these errors are dropped for most equations from now on.

Although this paper will not dwell on the detailed Kalman filtering equations, it provides the required steps to construct the filter model. Equations (25) and (28) below provide the full discretised system model used with a standard EKF construction. The first step in designing the filter is to identify the state vector x for equations of the model. For a tri-axial IMU, there are 3 orthogonally mounted accelerometers and 3 orthogonal gyroscopes. Since each axis has an unknown bias and an unknown scale factor, the calibration process consists of determining a total number of 12 unknowns. These unknowns are used as a part of the state vector to be estimated directly by the filter. In addition to the above unknown variables, linear velocities of the IMU in the Earth-fixed navigation frame, and the four-component quaternion vector constitute the state vector. A quaternion vector has been preferred over Euler angles to describe the attitude of the sensor in different maneuvering situations[4]. As a result, the state x can be constructed as a 19×1 vector, consisting of velocity, body attitude and stochastic errors (biases and scale factors) according to the following discrete-time representation:

$$x(k) = \begin{bmatrix} v^n(k) & q(k) & \beta_a^b(k) & \beta_g^b(k) & S_a^b(k) & S_g^b(k) \end{bmatrix}^T. \tag{12}$$

State Transition Model: The next step is to construct a discrete-time state transition model in the form of the following equation:

$$x(k) = f(x(k-1), u(k), w(k)). \tag{13}$$

where $u(k)$ and $w(k)$ denote the control input and the process noise respectively. The conditioned values obtained from Equations (8) and (9) are used as control inputs for the process model. Therefore, u is a 6×1 vector such that,

$$u(k) = \begin{bmatrix} \bar{a}_x^b(k) & \bar{a}_y^b(k) & \bar{a}_z^b(k) & \bar{\omega}_x^b(k) & \bar{\omega}_y^b(k) & \bar{\omega}_z^b(k) \end{bmatrix}^T. \tag{14}$$

Since the conditioned sensor measurements are still in the body-fixed frame, superscript 'b' is used for the vector components in (14). For constructing the discrete-time model, we first present the continuous-time equation models followed by the discretization process. The first set of equations of the state transition model (Equation (13)), links the rate of change of velocity to the state vector x, and the control inputs u according to

$$\dot{v^n} = a^n = C_b^n a^b + g^n \tag{15}$$

where $\bar{a}^b = \begin{bmatrix} \bar{a}_x^b & \bar{a}_y^b & \bar{a}_z^b \end{bmatrix}^T$ is formed by extracting the first three components of the control input vector in (14) and the 3×3 matrix C_b^n transforms the acceleration quantities in the body-fixed frame to the navigation frame. The gravity vector $g^n = \begin{bmatrix} 0 & 0 & g \end{bmatrix}^T$ with g denoting gravity, is used to compensate the effect of the local gravity on the measured acceleration along the Earth's z-axis. Substituting Equation (10) into (15) results in the velocity equations for the state transition model, that is

$$\dot{v^n} = C_b^n \left((1 + S_a^b) \circ \bar{a}^b \right) + C_b^n \beta_a^b + g^n. \tag{16}$$

where $\circ$ represents the Hadamard product as in [28]. This type of product (also known as the component-wise product) is between two matrices or vectors with the same dimensions[5]. C_b^n should be expressed in terms of the filter states (in this case, the quaternions). This is done by using the quaternion transformation as

$$C_b^n = \begin{bmatrix} q_0^2 + q_1^2 - q_2^2 - q_3^2 & -2(q_0 q_3 - q_1 q_2) & 2(q_0 q_2 + q_1 q_3) \\ 2(q_0 q_3 + q_1 q_2) & q_0^2 - q_1^2 + q_2^2 - q_3^2 & -2(q_0 q_1 - q_2 q_3) \\ -2(q_0 q_2 - q_1 q_3) & 2(q_0 q_1 + q_2 q_3) & q_0^2 - q_1^2 - q_2^2 + q_3^2 \end{bmatrix} \tag{17}$$

The second set of equations for the state transition model expresses the orientation of the IMU platform using gyro measurements,

$$\dot{q} = \frac{1}{2}[q\otimes]\check{\omega}_{nb}^b \tag{18}$$

where

$$[q\otimes] = \begin{bmatrix} q_0 & -q_1 & -q_2 & -q_3 \\ q_1 & q_0 & -q_3 & q_2 \\ q_2 & q_3 & q_0 & -q_1 \\ q_3 & -q_2 & q_1 & q_0 \end{bmatrix} \quad and \quad \check{\omega}_{nb}^b = \begin{bmatrix} 0 \\ \omega_x^b \\ \omega_y^b \\ \omega_z^b \end{bmatrix}. \tag{19}$$

Equation (18) expresses the rate of change of the quaternion in terms of the quaternion and angular velocities from the gyro. In this way, $\dot{q}$ is indirectly linked to the state vector x and control input u. Substituting Equation (11) into (18) results in the second set of equations for the state transition model, that is

$$\dot{q} = \frac{1}{2}[q\otimes] \left((1 + \check{S}_g^b) \circ \bar{\omega}_{nb}^b + \check{\beta}_g^b \right) \tag{20}$$

where $\bar{\omega}_{nb}^b$ is the modified angular velocity (extracted from the control input vector in (14)), according to

$$\bar{\omega}_{nb}^b = \begin{bmatrix} 0 & \bar{\omega}_x^b & \bar{\omega}_y^b & \bar{\omega}_z^b \end{bmatrix}^T \tag{21}$$

and similar to the notation used in Equation (19),

$$\check{S}_g^b = \begin{bmatrix} 0 & S_{\mathrm{g,x}}^b & S_{\mathrm{g,y}}^b & S_{\mathrm{g,z}}^b \end{bmatrix} \tag{22}$$

$$\check{\beta}_g^b = \begin{bmatrix} 0 & \beta_{\mathrm{g,x}}^b & \beta_{\mathrm{g,y}}^b & \beta_{\mathrm{g,z}}^b \end{bmatrix}. \tag{23}$$

The differential equations for the last 12 states in Equation (12) are simply:

$$\begin{bmatrix} \dot{\beta}_a^b & \dot{\beta}_g^b & \dot{S}_a^b & \dot{S}_g^b \end{bmatrix}^T = 0. \tag{24}$$

[4]Attitude parameterization using the quaternion is more computationally efficient and numerically accurate than the Euler angle method.

[5]Let A and B be $m \times n$ matrices with entries in C. The Hadamard product of A and B is defined by $[A \circ B]_{ij} = [A]_{ij}[B]_{ij}$ for all $1 \leq i \leq$ m, $1 \leq j \leq$ n.

This set of equations is based on the assumption that the stochastic errors of inertial sensors vary slowly compared to the dynamics of the moving vehicle. Hence, they are considered as constant values between two consecutive IMU samples throughout the EKF's prediction stage. As will be shown in the next section, these varying errors are estimated during each iteration of the filter. Equations (16), (18) and (24) are the fundamental equations that enable the computation of the state x of the sensor from an initial state $x(0)$ and a series of measurements $\tilde{a}^b$ and $\tilde{\omega}^b$. The salient point here is that these equation are valid for general motion of the IMU in 3D space, regardless of the motion. Since the discrete form of the EKF is used in this paper, the above continuous-time state transition model is discretised [27] using the forward Euler method [29]:

$$\begin{bmatrix} v^n(k) \\ q(k) \\ \beta_a^b(k) \\ \beta_g^b(k) \\ S_a^b(k) \\ S_g^b(k) \end{bmatrix} = \begin{bmatrix} v^n(k-1) \\ q(k-1) \\ \beta_a^b(k-1) \\ \beta_g^b(k-1) \\ S_a^b(k-1) \\ S_g^b(k-1) \end{bmatrix} + \begin{bmatrix} C_b^n(k)\left((1+S_a^b(k))\circ \bar{a}^b(k)\right) + (\Delta T)C_b^n(k)\beta_a^b(k) + g^n(k) \\ \frac{(\Delta T)}{2}[q\otimes(k)]\left((1+\check{S}_g^b(k))\circ \bar{\omega}_{nb}^b(k) + \check{\beta}_g^b(k)\right) \\ 0 \\ 0 \\ 0 \\ 0 \end{bmatrix} \tag{25}$$

where ΔT is the sampling time of the IMU.

Observation Model: The observation model is generally constructed in order to provide a relationship between the observations, the state vector and the control input according to the following equation:

$$z(k) = h(x(k), u(k), v(k)). \tag{26}$$

where $v(k)$ denotes the observation noise. The sensor's velocity in the earth-fixed navigation frame is used as the basis for constructing the observation model, that is

$$z(k) = \begin{bmatrix} v_x^n(k) & v_y^n(k) & v_z^n(k) \end{bmatrix}^T \tag{27}$$

In the proposed dynamic calibration method, the raw IMU data is collected for rotational movements of the sensor about several arbitrary axes where no translational movement is imposed on the sensor's center of mass[6]. Moreover, the calibration starts from the stationary mode with zero initial velocity. As a result of this specific scheme of motion (assuming the linear acceleration caused by manual rotation is negligible), velocity in the navigation frame can be considered equal to zero throughout the calibration process. Since in reality no measuring instrument is used to directly measure the velocity of the sensor in the navigation frame, the term "pseudo-velocity" is used for referring to the mentioned measurements. The pseudo-velocity measurements are used as the filter's observation, therefore

$$\forall k: \qquad z(k) = \begin{bmatrix} 0 & 0 & 0 \end{bmatrix}^T + v(k) \tag{28}$$

[6]The method does not require advanced maneuvers of the sensor. The IMU is simply held by hand and rotated around several arbitrary axes by delicate wrist movements.

It is important to note that Equation (28) is just the simple case of the general observation model described by Equation (27). In applications where the velocity of the sensor is known at each time, this velocity can be used to form the observation model in order to correct the estimated states from the prediction phase of the EKF. This will be shown in Section III where the designed calibration procedure is used as a basis to form the structure of a GPS/INS integrated system.

After the filter is initialised, it enters a loop as long as IMU measurements exist. At any given time (k), the EKF first predicts the state based upon the state estimate from the previous time $(k-1)$. Subsequently, pseudo-velocity observation at the current time is used for further correction of this prediction and to provide a better estimate of the system states. The estimated state and covariance are augmented with the mean and covariance of the process noise. Through this recursive solution of prediction and update, the EKF efficiently estimates the bias and scale factor errors presented in the inertial sensors.

III. Experimental Results

The inertial data was collected from a prototype IMU known as ThinIMU Micro[7]which is an extremely small and very thin inertial measurement unit with an on-board processor. ThinIMU Micro chip includes an integrated dual-axis gyro [IDG-300 Datasheet, InvenSense, Inc.] for X and Y axes, and a yaw-rate gyro [ADXRS610 Datasheet, Analog Devices Inc. 2007] for Z axis. It also includes a three axis accelerometer [MMA7340L Datasheet, Freescale Semiconductor, Inc., 2007]. Due to the miniature footprint and low price, it is ideal for applications like AutoMap with its size, weight and cost constraints and it can be easily integrated into a motion capturing suit or a navigation platform. This IMU is depicted in Figure 1.

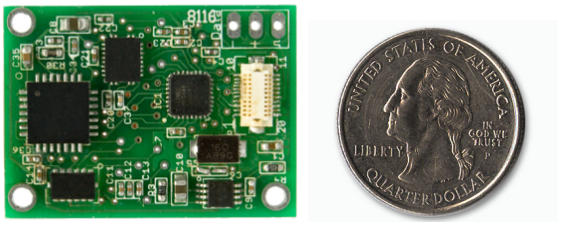

Figure 1: ThinIMU Micro consists of three accelerometers and three gyros in an orthogonal arrangement. (Dimensions: 31.5 × 25 × 5 (mm)).

The static calibration procedure outlined in Section II-A was performed to obtain the deterministic errors of the sensor. Removing the stochastic errors associated with the IMU was tested for both a stationary and a rotating IMU using the dynamic calibration algorithm described in Section II-B.

The left graph in Figure 2 illustrates the change in the roll and pitch angles for 10 data sequences before and after carrying out the dynamic calibration process. The measurements for all the sequences were collected from a static IMU,

[7] Designed and developed by Felix Schill at the School of Engineering, Australian National University.

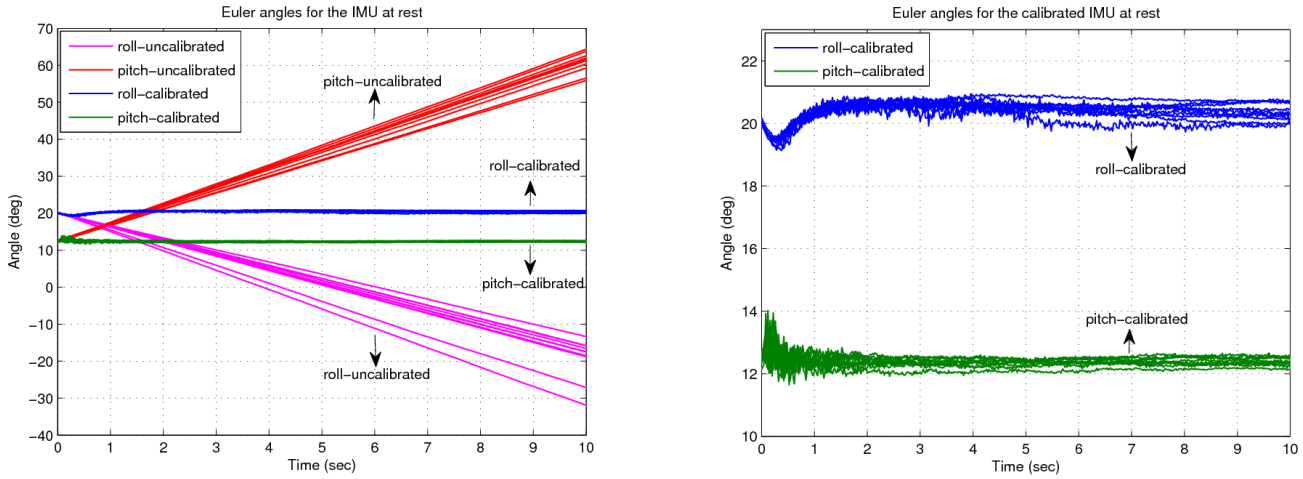

Figure 2: The roll and pitch angles of a stationary sensor with and without the dynamic calibration (left). The figure on the right is the enlarged view of the Euler angles for the dynamically calibrated sensor.

while the sensor was left unchanged on the table between two sequences. As can be seen from the figure, the attitude for the uncalibrated IMU diverges with time due to the bias terms presented in the sensor. Furthermore, there is a considerable difference between the attitude results of the uncalibrated IMU from sequence to sequence. This might be due to the variations of the turn-on bias which is an undesirable characteristic of MEMS IMUs. Consequently, it is crucial to remove the bias and scale factor errors associated with the sensor. As can be seen from the figure, the estimated Euler angles after performing the dynamic calibration phase using the pseudo-velocity concept are approximately fixed during the filter run. Figure 2 (right) is the enlarged view of the calibrated roll and pitch for all the data sequences.

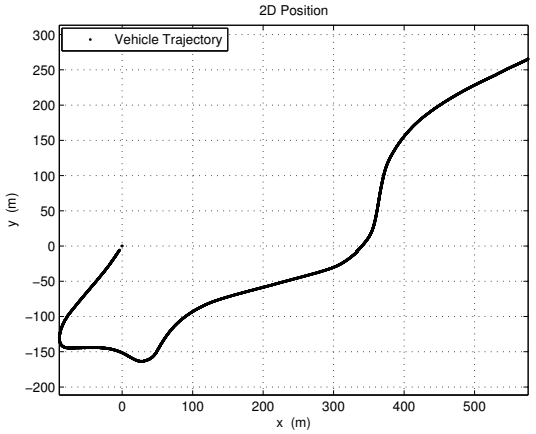

Figure 3: Test Vehicle's Trajectory

As the second contribution of this work, the calibration scheme described in this paper is applied to a designed GPS/INS integrated system comprising the ThinIMU Micro IMU and an ordinary GPS receiver. The development of the GPS/INS navigation system is enabled through the augmentation of the dynamic calibration method described in Section II-B. The integration system is designed by incorporating the developed EKF structure used to estimate the dynamic states of an IMU, with GPS velocity measurements. The main difference between this system and the calibration structure described in Section II-B is the use of GPS outputs instead of the so-called pseudo-velocity measurements as the EKF observed quantities according to

$$\forall k: \quad z(k) = \begin{bmatrix} V_x^{\mathrm{GPS}}(k) & V_y^{\mathrm{GPS}}(k) & V_z^{\mathrm{GPS}}(k) \end{bmatrix}^T + v_k \qquad (29)$$

The described GPS/INS algorithm was run on a data sequence collected by driving around a test vehicle on the trajectory shown in Figure 3. The path was chosen to include interesting types of vehicle motion for our navigation application (e.g. straight line, slight turn and sharp turn). The test vehicle is equipped with ThinIMU Micro and a Ublox 5 GPS antenna. Please note that since the physical distance between the two sensors is negligible in our setup, the velocity experienced by the IMU is considered to be the same as the GPS velocity. The GPS velocity updates of Equation (29), which are calculated directly from the GPS positioning information, correct and estimate the biases and scale factor errors presented in the IMU. In addition, the structure is capable of estimating the position, velocity and attitude (PVA) of the moving platform. The tuning process of the EKF is a crucial step in the fusion implementation. Tuning was performed by assigning appropriate values to the state covariance matrix (Q) and the observation covariance matrix (R)[8]. The effectiveness of the tuning process was verified by monitoring the velocity innovations and the normalised innovation square (NIS) as a measure of the filter's accuracy. Figure 4 compares the fusion system's performance for the calibrated and uncalibrated inertial sensors for a segment of the nominated trajectory. The behaviour of the accelerometer bias is illustrated in Figure 5. Other estimated errors are not shown here but they follow the same type of behaviour. Figure

[8]The exact value of all the tuning parameters are available from the authors on request.

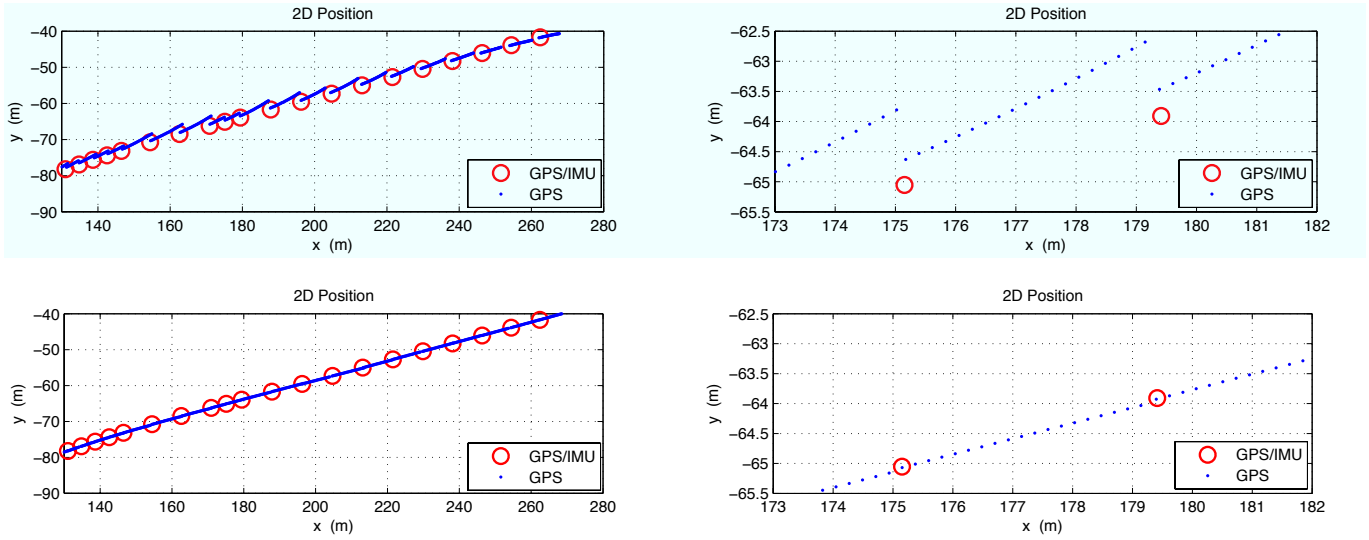

Figure 4: The GPS/INS integration results for uncalibrated (top) and calibrated (bottom) IMU. The figures at the right are the enlarged view of the left figures.

6 shows an example map output which is acquired by running the sign detection and the GPS/INS fusion algorithms on real data captured by the test vehicle. The estimated trajectory of the vehicle and the location of the detected road signs are illustrated.

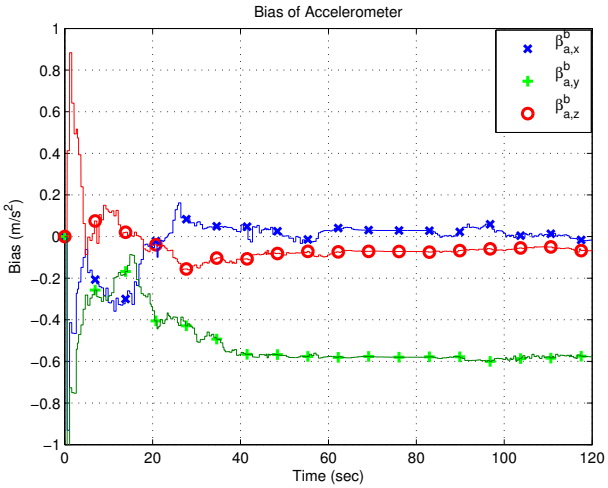

Figure 5: Stochastic biases of the accelerometer

IV. Conclusions and Future Work

A simple and effective calibration procedure was developed and tested successfully on a low-cost 6-DoF MEMS IMU. Pseudo-velocity measurements were utilised as the virtual observations for estimating the sensor's stochastic errors in the lab. The proposed method overcomes the most important deficiencies associated with previous work in the area.

The effectiveness of the calibration method was investigated through designing a GPS/MEMS-based IMU fusion system for outdoor applications. Although not presented in this paper, promising navigation results were attained for the GPS/INS integration for land vehicles under deliberate GPS dropout. The performance of the fusion system during GPS outage periods can be further improved using a nonlinear smoothing method [30]. Running the filtering algorithm both in forward and backward directions and combining the results using a smoother enables the fusion system to alleviate the sensor drifts.

Finally, the utilisation of ThinIMU Micro with the developed calibration procedure has enabled the AutoMap project to accurately localise survey vehicles and geo-locate the road signs of interests. The encouraging results merit further investigation into other application domains of the low-cost IMU under study. The calibration methodology discussed in this paper can potentially be used in other field applications with parsimonious consumption of resources.

References

[1] S. Godha, "Performance evaluation of low cost MEMS-based IMU integrated with GPS for land vehicle navigation application," *Master's thesis, Department of Geomatics Engineering, University of Calgary, Calgary, Canada*, 2006.

[2] L. Petersson. (2011) Nicta | automap. [Online]. Available: http://www.nicta.com.au/research/projects/AutoMap

[3] M. Grewal, V. Henderson, and R. Miyasako, "Application of Kalman filtering to the calibration and alignment of inertial navigation systems," *Automatic Control, IEEE Transactions on*, vol. 36, no. 1, pp. 3–13, 2002.

[4] E. Foxlin and L. Naimark, "Miniaturization, calibration & accuracy evaluation of a hybrid self-tracker," in *Mixed and Augmented Reality, 2003. Proceedings. The Second IEEE and ACM International Symposium on*. IEEE, 2003, pp. 151–160.

[5] E. Nebot and H. Durrant-Whyte, "Initial calibration and alignment of low-cost inertial navigation units for land vehicle applications," *Journal of Robotic Systems*, vol. 16, no. 2, pp. 81–92, 1999.

[6] A. Kim and M. Golnaraghi, "Initial calibration of an inertial measurement unit using an optical position tracking system," in *Position Location and Navigation Symposium, 2004. PLANS 2004*. IEEE, 2004, pp. 96–101.

[7] M. Park and Y. Gao, "Error analysis of low-cost MEMS-based accelerometers for land vehicle navigation," in *ION GPS 2002: 15 th*

Figure 6: Example map output. The resulted trajectory has been obtained using the GPS/MEMS IMU integration described in Section III. Location: Canberra, Australia (Source: Google Earth).

International Technical Meeting of the Satellite Division of The Institute of Navigation; Portland, OR. Institute of Navigation, 3975 University Drive, Suite 390, Fairfax, VA, 22030, USA,, 2002.

[8] Z. Syed, P. Aggarwal, C. Goodall, X. Niu, and N. El-Sheimy, "A new multi-position calibration method for MEMS inertial navigation systems," *Measurement Science and Technology*, vol. 18, p. 1897, 2007.

[9] J. Hall and R. Williams II, "Case study: Inertial measurement unit calibration platform," *Journal of Robotic Systems*, vol. 17, no. 11, pp. 623–632, 2000.

[10] D. Weston and D. Titterton, *Strapdown inertial navigation technology*. Lavenham Press Ltd, Lavenham, 1997.

[11] J. Farrell and M. Barth, *The global positioning system and inertial navigation*. McGraw-Hill Professional, 1999.

[12] E. Shin and N. El-Sheimy, "A new calibration method for strapdown inertial navigation systems," *Z. Vermess*, vol. 127, pp. 1–10, 2002.

[13] S. Sukkarieh, E. Nebot, and H. Durrant-Whyte, "A high integrity imu/gps navigation loop for autonomous land vehicle applications," *Robotics and Automation, IEEE Transactions on*, vol. 15, no. 3, pp. 572–578, 1999.

[14] M. Hadfield and K. Leiser, "Ring laser gyros come down to earth: field test results on the rlg modular azimuth position system (maps)," in *Position Location and Navigation Symposium, 1988. Record. Navigation into the 21st Century. IEEE PLANS'88., IEEE*. IEEE, 1988, pp. 61–72.

[15] W. Gao, Q. Nie, G. Zai, and H. Jia, "Gyroscope drift estimation in tightly-coupled ins/gps navigation system," in *Industrial Electronics and Applications, 2007. ICIEA 2007. 2nd IEEE Conference on*. IEEE, 2007, pp. 391–396.

[16] S. Winkler, M. Buschmann, T. Kordes, H. Schulz, and P. Vorsmann, "MEMS-based IMU development, calibration and testing for autonomous MAV navigation," in *Proceedings of the ION 59th Annual Meeting and the CIGTF 22nd Guidance Test Symposium (Albuquerque, NM, 23-25 Juni, 2003)*, pp. 128–134.

[17] R. Rogers, J. Wit, C. Crane III, D. Armstrong *et al.*, "Integrated INU/DGPS for autonomous vehicle navigation," in *Position Location and Navigation Symposium, 1996., IEEE 1996*. IEEE, 2002, pp. 471–476.

[18] P. Aggarwal, Z. Syed, X. Niu, and N. El-Sheimy, "Cost-effective testing and calibration of low cost MEMS sensors for integrated positioning, navigation and mapping systems," in *XXIII FIG (International Federation of Surveyors) Congress. Munich, Germany*, 2006.

[19] P. Aggarwal, Z. Syed, and N. El-Sheimy, "Thermal Calibration of Low Cost MEMS Sensors for Land Vehicle Navigation System," in *Vehicular Technology Conference, 2008. VTC Spring 2008. IEEE*. IEEE, 2008, pp. 2859–2863.

[20] M. El-Diasty and S. Pagiatakis, "Calibration and stochastic modelling of inertial navigation sensor errors," *Journal of Global Positioning Systems*, vol. 7, no. 2, pp. 170–182, 2008.

[21] I. Skog and P. Händel, "Calibration of a mems inertial measurement unit," in *XVII IMEKO World Congress on Metrology for a Sustainable Development, September*. Citeseer, pp. 17–22.

[22] O. Salychev and B. M. S. T. University, *Inertial systems in navigation and geophysics*. Bauman MSTU Press, 1998.

[23] F. Ferraris, U. Grimaldi, and M. Parvis, "Procedure for effortless in-field calibration of three-axis rate gyros and accelerometers," *Sensors and Materials*, vol. 7, pp. 311–311, 1995.

[24] J. Lötters, J. Schipper, P. Veltink, W. Olthuis, and P. Bergveld, "Procedure for in-use calibration of triaxial accelerometers in medical applications," *Sensors and Actuators A: Physical*, vol. 68, no. 1-3, pp. 221–228, 1998.

[25] S. Won and F. Golnaraghi, "A triaxial accelerometer calibration method using a mathematical model," *Instrumentation and Measurement, IEEE Transactions on*, vol. 59, no. 8, pp. 2144–2153, 2010.

[26] S. Sukkarieh, E. Nebot, and H. Durrant-Whyte, "Achieving integrity in an INS/GPS navigation loop for autonomous land vehicle applications," in *Robotics and Automation, 1998. Proceedings. 1998 IEEE International Conference on*, vol. 4. IEEE, 2002, pp. 3437–3442.

[27] J. Kim, *Autonomous navigation for airborne applications*. Dept. of Aerospace, Mechanical and Mechatronic Engineering, Graduate School of Engineering, University of Sydney, 2004.

[28] E. Million. (2011) The hadamard product. [Online]. Available: http://buzzard.ups.edu/courses/2007spring/projects/million-paper.pdf

[29] J. Butcher and E. Corporation, *Numerical methods for ordinary differential equations*. Wiley Online Library, 2008.

[30] J. Seo, J. Lee, C. Park, H. Lee, and S. Kim, "Application of nonlinear smoothing to integrated GPS/INS navigation system," *Journal of Global Positioning Systems*, vol. 4, no. 1-2, pp. 88–94, 2005.